Quantum Mechanical Calculations on Phosphate Hydrolysis Reactions

JOSE M. MERCERO,[1] PAUL BARRETT,[2] CHEUK W. LAM,[2] JOSEPH E. FOWLER,[1] JESUS M. UGALDE,[1] LEE G. PEDERSEN[2,3]

[1]*Kimika Fakultatea, Euskal Herriko Unibertsitatea, P.K. 1072, 20080 Donostia, Euskal Herria, Spain*
[2]*NIEHS, Research Triangle Park, North Carolina 27709*
[3]*Department of Chemistry, CB#3290, The University of North Carolina at Chapel Hill, Chapel Hill, North Carolina 27599-3290*

Received 16 April 1999; accepted 11 August 1999

ABSTRACT: Multiple biological processes are regulated by kinases and phosphatases. This study aims to provide nonenzymatic models for phosphorylation and dephosphorylation of serine, threonine, and tyrosine phosphate using *ab initio* guantum mechanical calculations. We reduce the problem to methyl phosphate hydrolysis to model serine/threonine, and the hydrolysis of phenyl phosphate to model the tyrosine. HF, B3LYP, and MP2 calculations with a 6-31+G(d) basis set were employed. The effect of water as a catalyst was also analyzed. As expected, the activation energy barrier is lowered.
 J Comput Chem 21: 43–51, 2000

Keywords: dephosphorylation; serine; threonine; reaction mechanism; *ab initio*

Introduction

The mechanism of the phosphorylation/dephosphorylation of hydroxyl-groups/phosphate-esters are of interest to many areas of biochemistry. The hormonal-initiated alteration of the activity of many enzymes is due to phosphorylation of the hydroxyl aminoacids serine and threonine.[1] The cellular signals for regulating cell growth, differentiation, and proliferation are, for instance, due to the phosphorylation of tyrosine in intracellular or membrane proteins.[2] Phosphate ester linkages are also responsible for the action of G-proteins in signal transduction, energy storage by ATP and GTP, and control of the formation of DNA and RNA.[3]

Consequently, a detailed description of the reaction:

$$[\mathrm{R{-}O{-}P(O_2){-}OH}]^- + \mathrm{H_2O} \rightleftharpoons \mathrm{ROH} + \mathrm{H_2PO_4^-} \quad (1)$$

could be useful in our quest to understand these biological processes. The general mechanism of these and related processes is the phosphorylation of Ser/Thr or Tyr (or the reverse reaction, which is the dephosphorylation of the *O*-phosphoaminoacids).

Correspondence to: K. Fakultatea; e-mail: ugalde@sg.chu.es
Contract/grant sponsor: Basque Government
Contract/grant sponsor: Spanish DGICYT; contract/grant number: PB96/1524
Contract/grant sponsor: Provincial Government of Gipukoa

CCC 0192-8651 / 00 / 010043-09

Several experimental studies concerning the enzymatic mechanism of these and similar reactions exist.[4–6] To study the reaction by theory, it is necessary to reduce the size of the problem. Our approach will be to base the mechanism on the reactivity of the metaphosphate anion, the existence of which was first proposed by Butcher et al.[7] and Barnard et al.[8] in 1955 as an intermediate in the hydrolysis of the phosphate ester bond:

$$[\mathrm{R{-}O{-}P(O_2){-}OH}]^- + \mathrm{H_2O} \rightleftharpoons \mathrm{ROH} + \mathrm{H_2O} + [\mathrm{PO_3}]^- \quad (2a)$$

$$\mathrm{H_2O} + [\mathrm{PO_3}]^- \rightleftharpoons \left[\mathrm{HO{-}P(O_2){-}OH}\right]^- \quad (2b)$$

Henchman et al.[9] found that Rxn 2b did not occur in the gas phase. Keesee and Castleman,[10] however, employing more flexible reactions conditions, were able to observe the transition from metaphosphate to orthophosphate.

In 1993, Wu and Houk[11] and Ma et al.[12] studied the problem theoretically. By utilizing the transition state for Rxn 2b proposed by Wu and Houk, we study the dephosphorylation of the phosphorylated hydroxyl aminoacids (serine, threonine, and tyrosine). To do so, we consider the functional part of the hydroxylaminoacids, for example, CH_3—OH for Ser/Thr and C_6H_5—OH for Tyr. The primary (Ser) vs. secondary (Thr) alcohol differences will be explored in a later work. Because these functional groups are phosphorylated, a more accurate representation would be: $[CH_3{-}O{-}P(O_2){-}OH]^-$ for Ser/Thr and $[C_6H_5{-}O{-}P(O_2){-}OH]^-$ for Tyr (see Fig. 1). As a preliminary calculation, we started from Rxn 3, then we substitute one of the hydrogens of the orthophosphate with a methyl (Rxn 4) or phenyl (Rxn 5) group to represent the corresponding *O*-phosphorylated hydroxyl aminoacid. Finally the catalytic effect of a molecule of water was also studied (Rxns 6–8, respectively). Note that the hash symbol implies a transitional state structure.

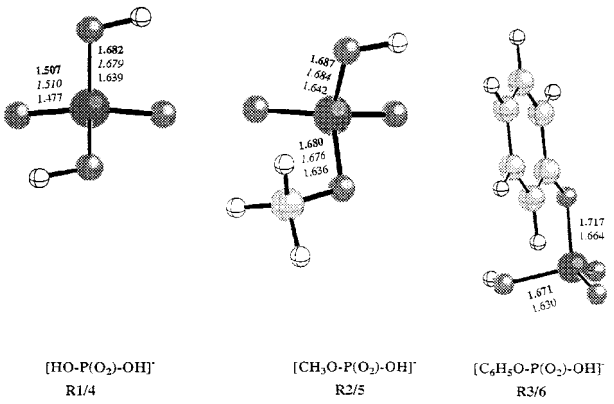

FIGURE 1. Reactants of Rxns 3–8. Bold-face distances correspond to B3LYP geometries, italic values to MP2, and normal font to HF (6-31+G*). Bond lengths are given in Å. Reactant 1/4 corresponds to our simplest model (Rxns 3 and 6). Reactant 2/5 is the model for the phospho-serine/threonine anion (Rxns 4 and 7). Reactant 3/6 is the model for phospho-tyrosine (Rxns 5 and 8).

$$[\mathrm{HO{-}P(O_2){-}OH}]^- \rightarrow \left[[\mathrm{H_2O{-}P(O_3)}]^-\right]^{\#} \rightarrow [\mathrm{PO_3{\cdot}H_2O}]^- \rightarrow \mathrm{H_2O} + [\mathrm{PO_3}]^- \quad (3)$$

$$[\mathrm{CH_3O{-}P(O_2){-}OH}]^- \rightarrow \left[[\mathrm{CH_3OH{-}P(O_3)}]^-\right]^{\#} \rightarrow [\mathrm{PO_3{\cdot}HOCH_3}]^- \rightarrow [\mathrm{PO_3}]^- + \mathrm{CH_3OH} \quad (4)$$

$$[\mathrm{C_6H_5O{-}P(O_2){-}OH}]^- \rightarrow \left[[\mathrm{C_6H_5OH{-}P(O_3)}]^-\right]^{\#} \rightarrow [\mathrm{PO_3{\cdot}HOC_6H_5}]^- \rightarrow [\mathrm{PO_3}]^- + \mathrm{C_6H_5OH} \quad (5)$$

$$[\mathrm{HO{-}P(O_2){-}OH}]^- + \mathrm{H_2O} \rightarrow \left[[\mathrm{H_2O{-}P(O_3){-}OH_2}]^-\right]^{\#} \rightarrow [\mathrm{PO_3{\cdot}2H_2O}]^- \rightarrow [\mathrm{PO_3}]^- + 2\mathrm{H_2O} \quad (6)$$

$$[\mathrm{CH_3O{-}P(O_2){-}OH}]^- + \mathrm{H_2O} \rightarrow \left[[\mathrm{CH_3OH{-}P(O_3){-}OH_2}]^-\right]^{\#} \rightarrow [\mathrm{PO_3{\cdot}H_2O{\cdot}HOCH_3}]^- \rightarrow [\mathrm{PO_3}]^- + \mathrm{CH_3OH} + \mathrm{H_2O} \quad (7)$$

$$[\mathrm{C_6H_5O{-}P(O_2){-}OH}]^- + \mathrm{H_2O} \rightarrow \left[[\mathrm{C_6H_5OH{-}P(O_3){-}OH_2}]^-\right]^{\#} \rightarrow [\mathrm{PO_3{\cdot}H_2O{\cdot}HOC_6H_5}]^- \rightarrow [\mathrm{PO_3}]^- + \mathrm{C_6H_5OH} + \mathrm{H_2O} \quad (8)$$

Methods

All calculations were performed with the GAUSSIAN94[13] package. HF, DFT, and MP2 (no frozen orbitals) calculations were performed for the smallest reactions studied in this work, that is, Rxns 3, 4, 6, and 7, while only HF and DFT methods were used for the larger systems, Rxns 5 and 8. The harmonic vibrational frequencies and the thermal energy corrections are evaluated at each level of theory.

Previously reported DFT calculations have shown accurate data comparable to those given by cpu-intensive electron-correlation methods.[14] However, these methods frequently overestimate bond dissociation energies.[15] The hybrid methods of HF and DFT theories often overcome this problem.[16] The Becke hybrid[17] (B3), combined with

TABLE I.
Calculated Energy Changes for Rxn 6 (Defined in Fig. 2) at Different Levels of Theory (kcal/mol).

Rxn 6	Rxn Energy	Activation Energy	Complexation Energy
HF/6-31+G*	28.06	31.59	5.26
MP2/6-31+G*	24.02	12.15	−3.57
B3LYP/6-31+G*	21.62	11.36	−3.17
B3LYP/6-311+G*	21.19	10.43	—
B3LYP/6-3l++G(2df,2p)	21.86	13.41	—
G2(MP2)	25.17	16.29	—

the correlation functionals reported by Lee, Yang, and Parr[18] (LYP), has been chosen for this work. In general, we find a good accordance between MP2 and B3LYP results (see Table I).

An all-electron 6-31G split valence basis set was used for all atoms. This basis set was augmented with a diffuse *sp*-set of functions and a set of polarizing *d*-orbitals (6D). The inclusion of *d*-orbitals was mandatory, because they govern the phosphorus reactivity of these species. We shall refer to this basis as 6-31+G(d). Larger basis set and the G2(MP2)[19] procedures were also used, and Rxn 6 chosen as a reference reaction to analyze basis set effects. As can be seen from Table I, the B3LYP/6-311+G(d), B3LYP/6-31++G(2df,2p), and the G2(MP2) results agree reasonably well with those from the MP2/6-31+G(d) and B3LYP/6-31+G(d) levels of theory.

The entropy changes and thermal corrections are evaluated using the standard expressions for an ideal gas in the canonical ensemble. Details can be found in McQuarrie[20] and other standard statistical mechanics texts.

Files for the coordinates of the relevant species are available from the author on request.

Results and Discussion

The calculated energies (the sum of the electronic and thermal energies) of the species involved in all six reactions are shown in Table II. The sum of the

TABLE II.
Sum of Electronic and Thermal Energies (in Hartrees) for the Species Involved in the Studied Reactions.

Species		HF/6-31+G*	B3LYP/6-31+G*	MP2/6-31+G*
$[HO—P(O_2)—OH]^-$	(R1/4)	−641.453320	−643.590504	−642.342831
$[[H_2O—P(O_3)]^-]^{\#}$	(TS1)	−641.377577	−643.541693	−642.291157
$[PO_3 \cdot H_2O]^-$	(I1)	−641.426508	−643.576201	−642.326706
$[[H_2O—P(O_3)—OH_2]^-]^{\#}$	(TS4)	−717.396455	−719.972586	−718.513343
$[PO_3 \cdot 2H_2O]^-$	(I4)	−717.435364	−719.992939	−718.535438
$[CH_3O—P(O_2)—OH]^-$	(R2/5)	−680.443708	−682.862943	−681.469009
$[[CH_3OH—P(O_3)]^-]^{\#}$	(TS2)	−680.369554	−682.815120	−681.418204
$[PO_3 \cdot HOCH_3]^-$	(I2)	−680.414850	−682.845969	−681.446544
$[[CH_3OH—P(O_3)—OH_2]^-]^{\#}$	(TS5)	−756.389336	−759.246185	−757.642901
$[PO_3 \cdot H_2O—HOCH_3]^-$	(I5)	−756.421965	−759.263192	−757.654618
$HOCH_3$		−114.982499	−115.670581	−115.309685
$[C_6H_5O—P(O_2)—OH]^-$	(R3/6)	−870.914549	−874.566362	—
$[PO_3 \cdot HOC_6H_5]^-$	(I3)	−870.892929	−874.556463	—
$[[C_6H_5OH—P(O_3)—OH_2]^-]^{\#}$	(TS6)	−946.854615	−950.946742	—
$[PO_3 \cdot H_2O \cdot HOC_6H_5]^-$	(I6)	−946.897212	−950.971392	—
C_6H_5OH		−305.451091	−307.370370	—
$[PO_3]^-$		−565.415502	−567.1564918	−566.115373
H_2O		−75.991990	−76.3986394	−76.188225

TABLE III.
Sum of the Electronic and Thermal Energies (H^0_{298} in Hartrees), and Entropy (S^0_{298}, cal/molK) of the Different Species.

		HF		B3LYP		MP2	
		H^0_{298}	S^0_{298}	H^0_{298}	S^0_{298}	H^0_{298}	S^0_{298}
$[HO—P(O_2)—OH]^-$	(R1/4)	−641.453320	71.31	−643.589560	73.06	−642.341886	72.79
$[[H_2O—P(O_3)]^-]^\#$	(TS1)	−641.376633	71.31	−643.540749	73.11	−642.290213	72.74
$[PO_3{\cdot}H_2O]^-$	(I1)	−641.425564	80.11	−643.575256	80.64	−642.325765	80.37
$[[H_2O—P(O_3)—OH_2]^-]^\#$	(TS4)	−717.395511	80.87	−719.971642	82.00	−718.512398	81.49
$[PO_3{\cdot}2H_2O]^-$	(I4)	−717.434420	97.50	−719.991995	97.17	−718.534494	97.74
$[CH_3O—P(O_2)—OH]^-$	(R2/5)	−680.442764	80.39	−682.861999	82.10	−681.468065	81.62
$[[CH_3OH—P(O_3)]^-]^\#$	(TS2)	−680.368610	80.5	−682.814176	82.94	−681.417262	81.81
$[PO_3{\cdot}HOCH_3]^-$	(I2)	−680.413906	96.15	−682.845025	95.61	−681.445599	94.28
$[[CH_3OH—P(O_3)—OH_2]^-]^\#$	(TS5)	−756.388391	88.79	−759.245240	90.22	−757.641957	88.75
$[PO_3{\cdot}H_2O{\cdot}HOCH_3]^-$	(I5)	−756.421021	112.88	−759.262248	110.13	−757.653674	110.76
$HOCH_3$		−114.981555	56.65	−115.669637	56.87	−115.308741	56.82
$[C_6H_5O—P(O_2)—OH]^-$	(R3/6)	−870.913605	97.65	−874.565418	99.93	—	—
$[PO_3{\cdot}HOC_6H_5]^-$	(I3)	−870.891985	107.46	−874.555519	108.96	—	—
$[[C_6H_5OH—P(O_3)—OH_2]^-]^\#$	(TS6)	−946.853671	106.97	−950.945798	110.13	—	—
$[PO_3{\cdot}H_2O{\cdot}HOC_6H_5]^-$	(I6)	−946.896267	125.08	−950.970447	123.51	—	—
C_6H_5OH		−305.450147	73.64	−307.369353	74.72	—	—
$[PO_3]^-$		−565.414558	62.87	−567.155547	62.13	−566.114429	62.15
H_2O		−75.991051	46.36	−76.397694	45.12	−76.187281	45.14

electronic and thermal enthalpies at 298 K and the entropy of the species are given in Table III, and Table IV collects the calculated relative energies, entropies, enthalpies, and Gibbs free energies of the reactions previously described.

REACTIONS 3 TO 6

Similar reaction pathways were found for the three reactants (Fig. 1). Processes 3/6 and 4/7 pass through a transition state (TS1 and TS2 in Fig. 2) and lead to an intermediate complex (I1 and I2 in Fig. 3) formed between the metaphosphate and the corresponding leaving group, and finally these complexes dissociate into the final products metaphosphate anion ($[PO_3^-]$) and H_2O (in Rxn 3) or CH_3OH (in Rxn 4). No transition state was found for Rxn 5, possibly due to the complexity of the multidimensional potential energy surface, or perhaps a different mechanism is involved. Apart from that, the same kind of complex was located for Rxn 5 (I3), which ultimately dissociates into phenol and metaphosphate. Although Figures 1–3 are given to depict the main reactants, transition states, and intermediates, Figure 4 provides the definitions used to describe the reaction paths, and together with Table IV will help in the understanding of the thermodynamics of these reactions.

For Rxn 3, the $[HO—P(O_2)—OH]^-$ anion forms a four-membered ring transition state. The bridging hydrogen migrates to the adjacent oxygen where the O—H breaking and the forming bond lengths are 1.266 and 1.216 at the B3LYP level of theory. Again, the geometries of B3LYP and MP2 agree reasonably well (see Fig. 2), and the HF bond lengths are slightly shorter than those given by the methods that include electron correlation. Thus, for simplicity, hereafter we will focus our discussion on the B3LYP geometries. As the hydrogen atom migrates, P—O bond elongation occurs (at the same oxygen that accepts the hydrogen) changing from 1.683 to 2.101 Å, and the remaining PO_3 portion is nearly planar.

The only difference between TS1 and TS2 is the substitution of one of the hydrogens for a methyl group, and as can be seen in Fig. 2, the geometries of both four-member rings are similar.

Transition states TS1 and TS2 are quite high in energy. For Rxn 3 the free-energy barriers are 47.94, 30.60, and 32.44 kcal/mol at the HF, B3LYP, and MP2 levels of theory, respectively, and these barriers are 46.50, 29.76, and 31.82 kcal/mol, respectively,

TABLE IV.

Calculated Changes in the Energy (ΔE^0_{298}, kcal/mol), Entropy (ΔS^0_{298}, cal/molK), Enthalpy (ΔH^0_{298}, kcal/mol) and Free Energy (ΔG^0_{298}, kcal/mol), where Activation (Step 1), Complexation (Step 2), and Reaction (Step 3) Thermodynamic Changes Are Defined in Figure 4.

	HF				B3LYP				MP2			
	ΔE^0_{298}	ΔS^0_{298}	ΔH^0_{298}	ΔG^0_{298}	ΔE^0_{298}	ΔS^0_{298}	ΔH^0_{298}	ΔG^0_{298}	ΔE^0_{298}	ΔS^0_{298}	ΔH^0_{298}	ΔG^0_{298}
Rxn 3												
Act. (**Step 1**)	47.53	−1.38	47.53	47.94	30.63	0.05	30.63	30.60	32.43	−0.06	32.43	32.44
Comp. (**Step 2**)	16.82	7.42	16.82	14.20	8.98	7.57	8.98	6.80	10.12	7.58	10.12	7.86
Rxn (**Step 3**)	28.76	38.54	29.35	17.86	22.20	34.19	22.79	12.59	24.62	34.49	25.21	14.93
Rxn 6												
Act. (**Step 1**)	30.66	−38.18	30.07	41.45	10.39	−36.18	9.80	20.58	11.12	−36.44	10.52	21.32
Comp. (**Step 2**)	6.24	−21.54	5.65	12.08	−2.38	−21.05	−2.98	3.29	−3.75	−20.19	−3.34	2.68
Rxn 4												
Act. (**Step 1**)	46.53	0.11	46.53	46.50	30.01	0.84	30.01	29.76	31.88	0.19	31.88	31.82
Comp. (**Step 2**)	18.11	15.76	18.11	13.41	10.65	13.51	10.65	6.62	14.10	12.66	14.10	10.32
Rxn (**Step 3**)	28.68	41.12	29.27	17.01	22.51	36.89	23.10	12.10	27.58	37.34	28.17	17.04
Rxn 7												
Act. (**Step 1**)	29.09	−37.96	28.50	39.82	9.66	−37.00	9.07	20.10	8.99	−38.01	8.40	19.74
Comp. (**Step 2**)	8.62	−13.87	8.03	12.16	−1.01	−17.10	−1.60	3.49	1.64	−16.00	1.05	5.82
Rxn 5												
Comp. (**Step 2**)	13.57	9.81	13.57	10.64	6.21	9.03	6.21	3.52	—	—	—	—
Rxn (**Step 3**)	30.09	40.86	30.69	18.50	24.79	36.92	25.43	14.42	—	—	—	—
Rxn 8												
Act. (**Step 1**)	32.58	−37.04	31.99	43.04	11.46	−34.93	10.86	21.28	—	—	—	—
Comp. (**Step 2**)	5.85	−18.93	5.26	10.91	−4.01	−21.54	−4.60	1.82	—	—	—	—

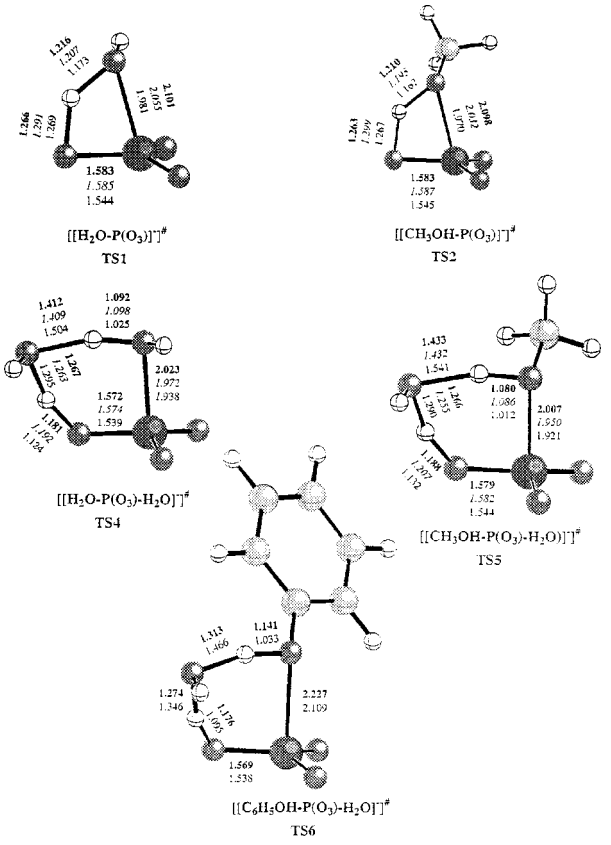

FIGURE 2. Transition states for Rxns 3, 4, 6, 7, and 8. Bold-face distances correspond to B3LYP geometries, italic values to MP2, and normal font to HF (6-31+G*). Bond lengths are given in Å.

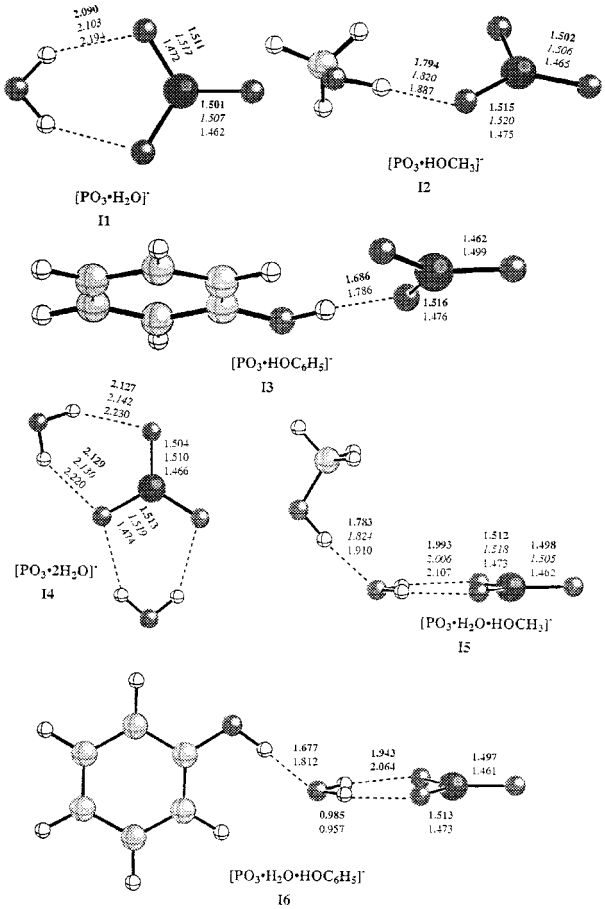

FIGURE 3. Intermediate complexes of Rxns 3–8. Bold-face distances correspond to B3LYP geometries, italic values to MP2, and normal font to HF (6-31+G*). Bond lengths are given in Å.

for Rxn 4. (Recall that we do not have the barrier for Rxn 5, because we were not able to locate the corresponding transition state.) A large difference is apparent between the HF level of theory and B3LYP/MP2 levels, while the data obtained with the latter two levels of theory are in good accordance with each other. We can compare this barrier with the highest level of theory employed by Wu and Houk[11] MP4/6-31+G**//HF/6-31+G(*), which found a barrier of 33.10 kcal/mol for Rxn 3, a value between our HF and correlation methods. Blades et al.[21] determine this barrier energy experimentally from kinetic energy thresholds for the collision-induced decomposition of $[H—O—P(O_2)—OH]^-$. The value they obtained was ca. 54 kcal/mol, which is much higher than the theoretical values. However, the authors did express concerns about the appropriateness of using the RRKM methodology to estimate the barrier.

These transition states, instead of dissociating directly to the final products, lead to a complex in the three reactions (I1, I2, and I3 in Fig. 3). A detailed mechanism for the transition from TS1 to I1 is given by Ma et al.;[12] this may possibly be extendible to Rxn 4 (and 5 if a transition state were involved). TS1 leads to an hydrogen bonded intermediate (I1) with C_{2v} symmetry, formed by metaphosphate anion and a molecule of water. The two hydrogens of the water molecule are directed towards two oxygens of the metaphosphate anion, and the bond length in the B3LYP level of theory is 2.090 Å. This intermediate (I1) is at 6.80 kcal/mol free energy above the reactant, and it dissociates to the products metaphosphate and water, which are about 5.8 kcal/mol above this intermediate.

The intermediate in Rxn 4 (I2 in Fig. 3) is an asymmetric complex, for which the hydrogen of the methanol is hydrogen bound to one of the oxygens of the metaphosphate, at 1.794 Å. This complex is 6.62 kcal/mol in free energy above the reac-

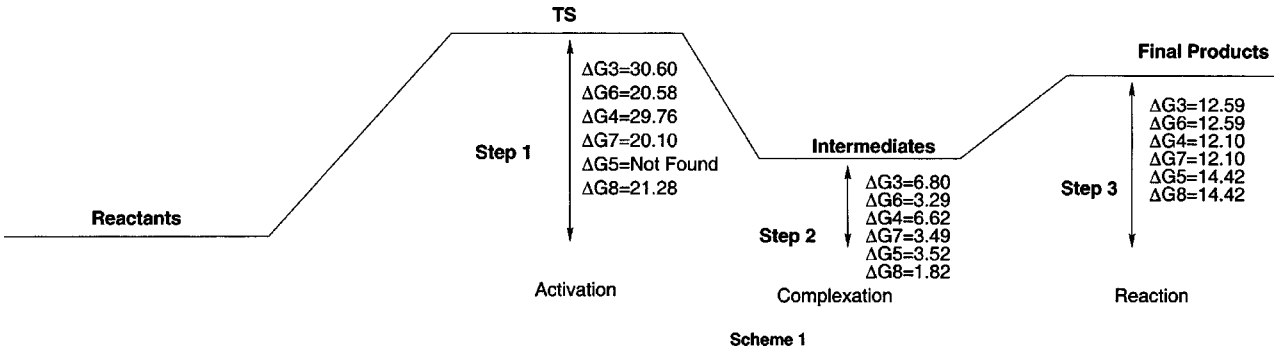

FIGURE 4. Scheme 1 represents the reaction path for Rxns 3–8. The free-energy changes of the corresponding step are given in kcal/mol, at the B3LYP level of theory.

tants. Ultimately, I2 dissociates into methanol and metaphosphate anion, which are about 5.5 kcal/mol above the intermediate. A C_s symmetry structure was also located, for which the metaphosphate and the OH group of the methanol were in the same plane, but this isomer had an imaginary frequency (corresponding to rotation around the hydrogen bond). For Rxn 5 a C_s hydrogen-bonded complex formed between the phenol and the metaphosphate anion was found (I3 in Fig. 4) at 3.52 kcal/mol in free energy above the reactants.

The total reaction free energies are 17.86 (HF), 12.59 (B3LYP), and 14.93 (MP2) for Rxn 3; 17.01 (HF), 12.10 (B3LYP), and 17.04 (MP2) for Rxn 4; and 18.50 (HF) and 14.42 (B3LYP) kcal/mol for Rxn 5.

The reverse reactions of 3 and 6 have been widely studied, both experimentally and theoretically as a hydration of metaphosphate problem. Keese and Castleman[10] (KC) measured the standard enthalpy, entropy and free-energy changes for the addition of water to the metaphosphate in gas phase.

$$PO_3^-(\cdot H_2O)_n + H_2O \rightarrow PO_3^-\cdot(n+1)H_2O \qquad n = 0, 1 \quad (9)$$

From the data we have, we can compare our results for Rxn 9 ($n = 0$) with the experimental values. KC report -22.2 ± 1 cal/molK and -12.9 ± 0.3 kcal/mol for ΔS^0 and ΔH^0, respectively, while we obtain $\Delta S^0 = -29.12$ (HF), -26.6 (B3LYP), and -26.9 (MP2) cal/molK and $\Delta H^0 = -12.52$ kcal/mol (HF), -13.81 (B3LYP), and -15.09 (MP2) kcal/mol. Theory is in reasonable agreement with experiment. The ΔS^0 value is overestimated at every level of theory, which is not surprising, as the calculated frequencies have not been scaled and the HF and B3LYP ΔH^0 lie slightly to either side of the experimental value. As expected, we obtained the same results obtained by Wu and Houk[11] at the same level of theory. Ma et al. also calculated the ΔH^0 of this reaction at the HF/DZP+diff, CISD/DZP+diff, and CCSD/DZP levels of theory, with values of 18.4, 16.5, and 12.9 kcal/mol, respectively, which are also in good agreement with our predictions.

REACTIONS 6 TO 8

In Rxns 6 to 8, an additional water molecule has been added, and its catalytic effect analyzed. The three reactions follow the same reaction pathway as Rxns 3 and 4. A transition state is overcome to lead a complex, and then this complex dissociates into the corresponding products.

The presence of a water molecule stabilizes these transition states by donating a hydrogen to the leaving entity and at the same time accepting the hydrogen of the PO_3H moiety. The presence of an additional oxygen atom provides a new center about which the bond-breaking/bond-forming can occur. This makes for a much less geometrically strained transition state, and also provides an additional center for redistribution of charge.

The transition states (TS4, TS5, and TS6 of Fig. 2) have six-membered rings, for which two molecules of water tend to separate from the PO_3 moiety. The breaking P—O bond lengths are 2.023, 2.007, and 2.227 Å for TS4-6, respectively, and the breaking O—H bond distances, 1.181, 1.188, and 1.176 Å, respectively, at the B3LYP level of theory.

The addition of a molecule of water in Rxn 6 reduces the TS free-energy barrier of Rxn 3 from 30.60 to 20.58 kcal/mol, and from 29.76 to 20.10 kcal/mol in Rxn 7, at the B3LYP/6-31+G* level of theory, while for Rxn 8, a transition state was located which is 21.28 kcal/mol higher in free energy than the reactants energy.

These transition states also lead to some intermediate complexes, I4, I5, and I6 (see Fig. 3). In Rxn 6, TS4 leads to a the I4 complex formed by the

metaphosphate, and both water molecules with C_{2v} symmetry. Three other isomers of I4 were also located, with slightly different energies, but within a range of 1.5 kcal/mol, and this small energy differences is not relevant for the discussion of Rxn 6; therefore, we consider only the isomer with the lowest energy, I4. This intermediate leads to the products metaphosphate anion and two water molecules, which are 9 kcal/mol in free energy above the intermediate. Intermediates were also located for Rxns 7 and 8. Although both water molecules in I4 interact with the metaphosphate anion, the alcohol hydrogens of I5 and I6 form a hydrogen bond with the oxygen of the water molecule with bond lengths of 1.783 and 1.677 Å, respectively, and the water hydrogens hydrogen bond with two oxygens of the metaphosphate, forming a chain complex. These two complex types, however, are energetically very similar, I4 is 3.29 kcal/mol above the reactants, and I5 and I6 are located 3.49 and 1.82 kcal/mol above the reactants, respectively.

Keesee and Castleman also reported the enthalpy (-11.4 ± 0.2 kcal/mol) and entropy (-22.00 ± 1 cal/molK) changes of the second hydration step (Rxn 9 with $n = 1$). From our calculations, we obtain -11.95 kcal/mol and -28.61 cal/molK, respectively, at the B3LYP level of theory, in moderate agreement with the experiment.

Conclusions

Transition states corresponding to hydrolysis of dihydrogen orthophosphate, methyl-orthophosphate, and phenyl-orthophosphate were found by modeling Wu and Houks transition states[11] for the hydrolysis of dihydrogen orthophosphate to water and metaphosphate anion with and without a water catalyst. HF, MP2, and B3LYP methods were used, and a good accordance between MP2 and B3LYP methods was observed.

Methyl-phosphate was used to model *O*-phosphoserine/threonine, and orthophenyl-phosphate for *O*-phosphotyrosine. This model proceeds via transition state to an intermediate complex, and finally dissociates into orthophosphate and the corresponding alcohol. The transition state barrier is lower when a water molecule is introduced as a catalyst; this suggests that enzymatic reactions of serine or threonine *in vivo* would utilize a water or a water-like molecule. However, this activation barrier is still fairly large, and it must be that other interactions than we have considered here will lower the barrier in enzymatic reactions.

The energetics of the various reactions is relatively independent of the leaving group in the cases studied (—OH, —OCH_3, —OC_6H_5). Reactions 3 and 4 must pass through a transition state with a barrier of 27.93 and 26.69 kcal/mol, respectively, and Rxns 6, 7, and 8 have barriers of 20.09, 19.6, and 19.77 kcal/mol, respectively.

For the phenyl phosphate model, no transition state was located for Rxn 5; while adding a water molecule as a catalyst, a transition state was found that may indicate that a different path is involved or that due to the system complexity, we have not yet been able to locate the transition state for Rxn 5.

This study provides an understanding for the mechanisms of the phosphorylation and dephosphorylation of simple phosphate esters and the role of water in the hydrolysis process. Other studies have reported experimental transition state structures in phosphatase catalysis with complex biological enzymes.[5, 6] For example, a nearby aspartate side chain is thought to provide a proton to stabilize the leaving group in phosphatase activity toward small phosphate monoesters[5, 6] with assumed concomitant lowering of the activation energy below our estimates for the uncatalyzed or water catalyzed steps. Our transition states have indicated that simplified models are sufficient starting structures for the modeled reactions. This approach can hopefully be used as a benchmark for future studies of biological reactions involving phosphate hydrolysis or esterification.

Acknowledgments

J.M.M. would like to thank LGP, his group, and CSJ students for the help, support, and hospitality offered during his stay in Chapel Hill. C.L. and P.B. were advanced undergraduate summer students at the NIEHS. We acknowledge computer suport from the North Carolina Supercomputing Center.

References

1. Mathews, C. K.; Holde, K. E. v. Biochemistry; The Benjamin/Cummings Publishing Company Inc.: Menlo Park, CA, 1996.
2. Fauman, E. B.; Yuvaniyama, C.; Schubert, H. L.; Stuckey, J. A.; Saper, M. A. J Biol Chem 1996, 271, 18780.
3. Florian, J.; Warshel, A. J Am Chem Soc 1993, 115, 11169.
4. Zhang, Z. Y.; Dixon, J. E. Adv Enzymol Relat Areas Mol Biol 1994, 68, 1.
5. Zhang, Z. Y.; Wu, L.; Chen, L. Biochemistry 1995, 34, 16088.

6. Denu, J. M.; Lohse, D. L.; Vijayalakhmi, J.; Saper, M. A.; Dixon, J. E. Proc Natl Acad Sci USA 1996, 93, 2493.
7. Butcher, W. W.; Westheimer, F. H. J Am Chem Soc 1955, 77, 2420.
8. Barnard, P. W. C.; Bunton, C. A.; Llewellyn, D. R.; Oldhamn, K. G.; Silver, B. L.; Vernon, C. A. Chem Ind (Lond) 1955, 760.
9. Henchman, M. J.; Viggiano, A. A.; Paulson, J. F.; Freedman, A.; Wormhoadt, J. J Am Chem Soc 1985, 107, 1453.
10. Keesee, R. G.; Castleman, A. W. J. J Am Chem Soc 1989, 111, 9015.
11. Wu, Y.; Houk, K. N. J Am Chem Soc 1993, 115, 11997.
12. Ma, B.; Xie, Y.; Shen, M.; Shleyer, P. v. R.; Schaefer, H. F.; J Am Chem Soc 1993, 115, 11169.
13. Frisch, M. J.; Trucks, G. W.; Schlegel, H. B.; Gill, P. M. W.; Johnson, B. G.; Robb, M. A.; Cheeseman, J. R.; Keith, T.; Petersson, G. A.; Montgomery, J. A.; Raghavachari, K.; Al-Laham, M. A.; Zakrzewski, V. G.; Ortiz, J. V.; Foresman, J. B.; Peng, C. Y.; Ayala, P. Y.; Chen, W.; Wong, M. W.; Andres, J. L.; Replogle, E. S.; Gomperts, R.; Martin, R. L.; Fox, D. J.; Binkley, J. S.; Defrees, D. J.; Baker, J.; Stewart, J. P.; Head-Gordon, M.; Gonzalez, C.; Pople, J. A. GAUSSIAN94 b.2; Gaussian, Inc., Pittsburgh, PA, 1995.
14. Labanowsky, J.; Andelzelm, J. Density Functional Methods in Chemistry; Springer Verlag: New York, 1991.
15. Tschinke, V.; Ziegler, T. Theor Chim Acta 1991, 81, 651.
16. Johnson, B.; Gill, P.; Pople, J. J Chem Phys 1993, 98, 5612.
17. Becke, A. J Chem Phys 1993, 98, 5648.
18. Lee, C.; Yang, W.; Parr, R. Phys Rev B 1988, 37, 785.
19. Curtis, L. A.; Raghavachari, K.; Pople, J. A. J Chem Phys 1993, 98, 1293.
20. McQuarrie, D. A. Statistical Thermodynamics; Harper and Row: New York, 1973.
21. Yeunghaw, A. T. B. H.; Kebarle, P. J Am Chem Soc 1996, 118, 196.